J Mater Sci (2012) 47:267–271
DOI 10.1007/s10853-011-5794-z

Microstructural and mechanical characterization of an ultra-high-strength $Fe_{86.7}Cr_{4.4}Mo_{0.6}V_{1.1}W_{2.5}C_{4.7}$ alloy

J. Hufenbach · S. Kohlar · U. Kühn · L. Giebeler · J. Eckert

Received: 24 March 2011 / Accepted: 12 July 2011 / Published online: 23 July 2011

Abstract This study describes the correlation between microstructure and mechanical properties of an ultra-high-strength $Fe_{86.7}Cr_{4.4}Mo_{0.6}V_{1.1}W_{2.5}C_{4.7}$ (at.%) alloy manufactured under high cooling rates and pure conditions. The applied preparation conditions promote the formation of non-equilibrium phases such as martensite, retained austenite and special carbides already in the as-cast state. The carbides form a 3-dimensional skeleton-like structure between the retained austenite and the martensite. This hard and finely ramified carbide network distributed throughout the entire ingot is a specific characteristic of this alloy and important for its excellent mechanical properties. The material exhibits extremely high engineering compression strength of almost 5500 MPa combined with a large compression strain of about 23% due to deformation-induced martensite formation. Furthermore, the alloy possesses a high hardness and tensile strength in the as-cast condition. This combination of mechanical properties leads to an outstanding engineering material for a variety of structural applications in the automotive and tool manufacturing industry.

J. Hufenbach (✉) · S. Kohlar · U. Kühn · L. Giebeler · J. Eckert
IFW Dresden, Institute for Complex Materials, Helmholtzstraße 20, 01069 Dresden, Germany
e-mail: j.k.hufenbach@ifw-dresden.de

S. Kohlar · L. Giebeler · J. Eckert
TU Dresden, Institute of Materials Science, Helmholtzstraße 7, 01069 Dresden, Germany

Introduction

The increasing demand in the automotive and tool manufacturing industries for innovative steels with high strength, hardness, wear resistance and large ductility, which exhibit an extreme mechanical loading capacity, stimulated the development of ultra-high-strength steels [1, 2]. This group of steels generally exhibits yield strengths exceeding 550 MPa [3] and tensile strengths of more than 700 MPa [1, 4]. However, ultra-high-strength materials are also exposed to tensile as well as compressive stresses or pure compressive load in use. For such applications, an ultra-high-strength iron-based $Fe_{86.7}Cr_{4.4}Mo_{0.6}V_{1.1}W_{2.5}C_{4.7}$ (at.%) alloy has been developed, which possesses a similar composition, wear resistance and hardness like a high speed steel (HSS) [5–7], but shows significantly higher compressive strength [8] in combination with good tensile properties. Another difference to commercial HSS and ultra-high-strength steels is that these classes of steels have to undergo complex manufacturing processes, which imply, e.g. costly heat treatments or thermo-mechanical rolling after the casting process [9–11], whereas the mechanical properties of the presented iron-based alloy can be generated already in the as-cast state. Therefore, a preparation method similar to that of bulk metallic glasses, implying high cooling rates and pure conditions, was used [12, 13]. Thereby a microstructure composed of martensite, retained austenite and a fine network of special carbides can be obtained [12, 14]. In the case of $Fe_{88.9}Cr_{4.3}V_{2.2}C_{4.6}$ (at.%), manufactured under such preparation conditions, an engineering compression strength of almost 4000 MPa together with a large compression strain of about 20% could be achieved [12]. Furthermore, the $Fe_{88.9}Cr_{4.3}V_{2.2}C_{4.6}$ alloy shows a superior mechanical behaviour under dynamic loading conditions and the

transformation-induced plasticity (TRIP) effect was verified [12, 14]. For further improvement of the mechanical properties, the composition of the alloy was slightly modified by adding small amounts of molybdenum and tungsten as carbide formers at the expense of the strong carbide former vanadium. For the new $Fe_{86.7}Cr_{4.4}Mo_{0.6}V_{1.1}W_{2.5}C_{4.7}$ alloy, this leads to a more complex and finer carbide network compared with the starting composition $Fe_{88.9}Cr_{4.3}V_{2.2}C_{4.6}$, whereas the transformation of retained austenite into martensite is still observable.

In this study, the correlation between the microstructure and the mechanical properties of the new developed high-strength $Fe_{86.7}Cr_{4.4}Mo_{0.6}V_{1.1}W_{2.5}C_{4.7}$ alloy modification is investigated. Thereby, the relationship between the non-equilibrium nature of the microstructure and the resulting mechanical properties is analysed, with special emphasis on the influence of the TRIP effect on the mechanical performance under quasi-static compressive loading.

Experimental

The $Fe_{86.7}Cr_{4.4}Mo_{0.6}V_{1.1}W_{2.5}C_{4.7}$ alloy was prepared by induction melting (Balzers) of the high purity elemental constituents (99.99 wt%) under an argon atmosphere using a ceramic crucible. After reaching the casting temperature of about 1823 K, the melt was cast into a copper mould with inner dimensions of $70 \times 120 \times 14$ mm^3. For obtaining the desired microstructure and phases (martensite, retained austenite and carbides), a cooling rate of about 10–50 K/s has to be achieved [15]. The actual composition of the ingots was verified by chemical analysis, i.e. the carbon content was measured by carrier gas hot extraction (CGHE, EMIA 820 V, Horiba) and for the elements Fe, Cr, Mo, V and W inductively coupled plasma optical emission spectrometry (ICP-OES; IRIS Intrepid II XUV, Thermo Fisher Scientific) was used. Table 1 displays the average carbon content and the standard deviation (SD) determined from five measurements as well as the average element contents and the SD resulting from fourfold ICP-OES measurement. Thereby no significant differences within the scope of precision could be detected. Furthermore, the nominal composition of the ingot and the element contents, which were determined experimentally, demonstrate a good correlation.

Microstructural analysis of the as-cast and deformed samples was performed by optical microscopy (OM; Epiphot 300, Nikon) and scanning electron microscopy (SEM; Leo 1530 Gemini, Zeiss). The samples for the OM observations of the as-cast state were etched with Beraha I. For the visualisation of the complex structured carbides in the alloy, the samples were deep etched (5 g $FeCl_3$, 10 mL HNO_3, 3 mL HCl, 87 mL C_2H_6O) and examined by SEM.

X-ray diffraction (XRD; STOE Stadi P, Mo $K_{\alpha 1}$ radiation) was used for structural characterization and phase identification in combination with a Rietveld analysis [16] using Fullprof [17].

Rockwell macrohardness measurements and room temperature compression and tensile tests were performed to study the mechanical behaviour of the alloy. The Rockwell macrohardness tests were conducted with a CV Instruments hardness tester using a test load of 1471 N. The quasi-static compression and tensile tests were carried out at a strain rate of 10^{-3} s^{-1} using an Instron 8562 testing device. For the compression tests, cylindrical and coplanar samples with dimensions of 3 mm diameter and 6 mm length were used. Five samples were deformed until fracture and three further specimens were deformed until a certain compression strain (0, 4, 9, 14 and 24%) was reached, such as to verify the TRIP effect. Subsequently, test pieces with a thickness of about 1 mm were cut out of an undeformed and the deformed specimens and the volume fraction of martensite was determined by a vibrating sample magnetometer (VSM 7300, Lake Shore Cryotronics).

For the tensile tests, five rectangular dog-bone-shaped samples after DIN 50125 were prepared. The specimens had a thickness of 1.4 mm, a sample width of 5 mm, a gauge length of 30 mm and a total length of 97 mm.

Results and discussion

Figure 1 presents a typical XRD pattern for an as-cast $Fe_{86.7}Cr_{4.4}Mo_{0.6}V_{1.1}W_{2.5}C_{4.7}$ sample. The alloy is mainly composed of a martensitic phase (m) and an austenitic (a) phase. These two phases are indexed on the basis of the structure models described by Kohlhaas et al. (martensite) [18] and Ridley et al. [19]. The lattice parameter a of (m) is refined to 2.888(2) Å and of (a) to 3.625(3) Å. The significantly larger lattice parameter for (m) is explained by

Table 1 Results of ICP-OES analysis and CGHE with standard deviation compared with the nominal composition of the presented alloy

	Fe	Cr	Mo	V	W	C
Nominal (wt%)	84.9	4.01	1.010	0.983	8.06	0.990
Experimental (wt%)	85.4	3.99	1.080	1.000	8.08	0.974
SD (wt%)	0.3	0.02	0.005	0.007	0.04	0.009

chromium as dopant, which leads to an increase of *a*. Energy dispersive X-ray spectroscopy measurements in the SEM (not shown here) confirm the existence of the chromium rich martensitic phase. The reflections of the both iron phases are broadened, indicating large distortions due to the special preparation conditions of the alloy. Furthermore, the XRD pattern indicates the existence of a mixed metal carbide c* with the general composition M_2C (M = Mo and/or W). However, the low phase content of almost 3 wt% is problematic for the correct indexing of the structure. Most plausible structure models in M_2C suitable for the determination of the carbide in the X-ray pattern in Fig. 1 are found for the space groups *Pbcn* [20] and $P\bar{3}1m$ [21]. A Mo_2C structure with the space group $Pca2_1$ [22] may be an additional candidate, but is discarded. This decision is supported by the existence of isostructural compounds for M_2C with either molybdenum or tungsten as metal ion in both space groups *Pbcn* and $P\bar{3}1m$. The M_2C compound with the space group $Pca2_1$ is, to our knowledge, just found for the molybdenum case. Mo_2C and W_2C are both found separately as well as closely associated, which leads to the assumption that the formation of a mixed $(Mo,W)_2C$ compound is very probable.

Figure 2a, b and c display the microstructure of the as-cast specimens. The optical microscope image obtained after etching with Beraha I (Fig. 2a) reveals that the material possesses a dendritic structure over the cross section of the ingot. The dendrites are mainly composed of martensite (dark phase) as well as fine carbides. Retained austenite and coarse carbides (light phases) are found in the interdendritic areas. The coexistence of the three phases (martensite, austenite and carbides) agrees well with the XRD results.

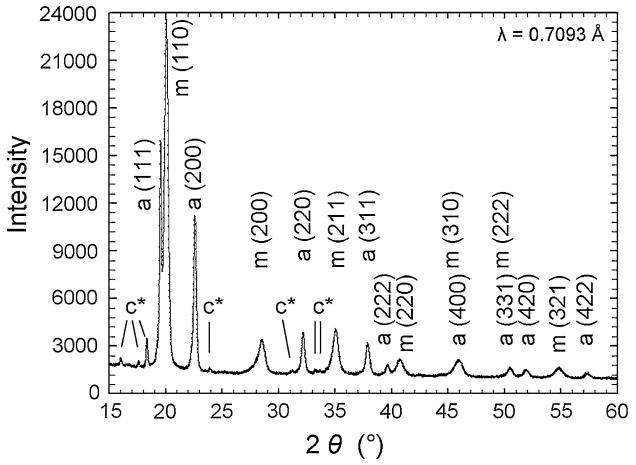

Fig. 1 XRD pattern of the as-cast $Fe_{86.7}Cr_{4.4}Mo_{0.6}V_{1.1}W_{2.5}C_{4.7}$ alloy with indexed martensitic (m) and austenitic (a) phase as well as M_2C (c*) with M = Mo and/or W

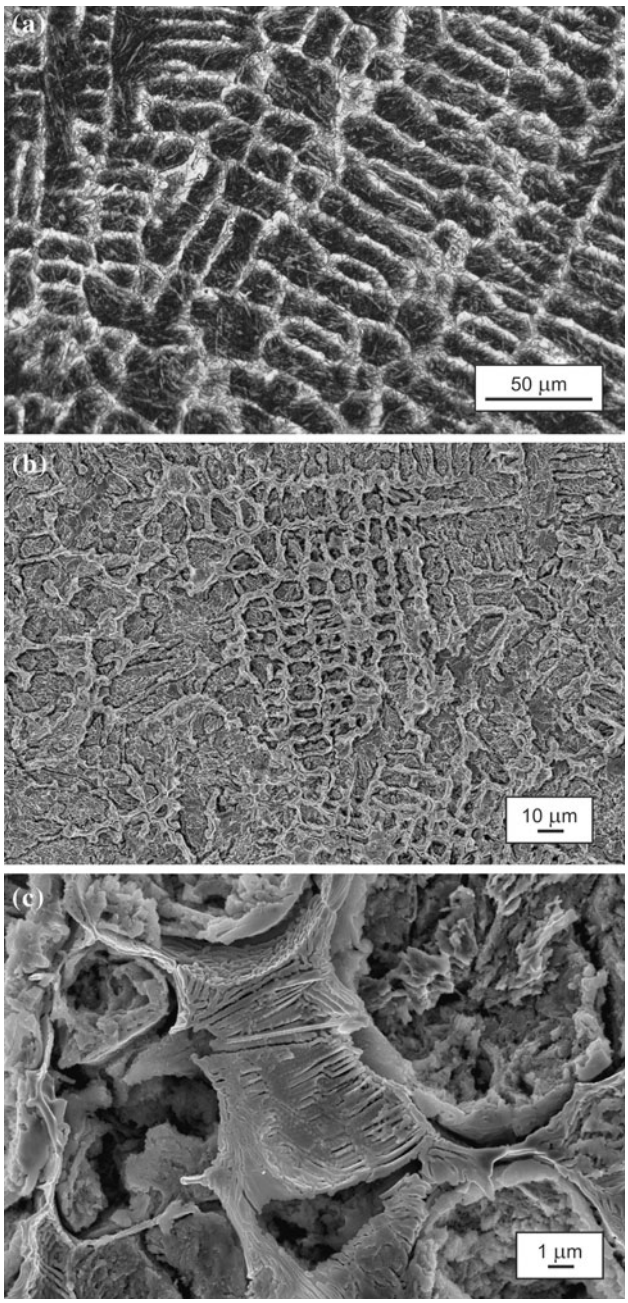

Fig. 2 **a** Optical micrograph of the dendritic structure of the as-cast $Fe_{86.7}Cr_{4.4}Mo_{0.6}V_{1.1}W_{2.5}C_{4.7}$ alloy showing the distribution of the present phases; **b**, **c** SEM images of the $Fe_{86.7}Cr_{4.4}Mo_{0.6}V_{1.1}W_{2.5}C_{4.7}$ alloy illustrating the fine network-like structure formed by complex carbides and its arrangement within the material

Figure 2b and c show SEM images of the $Fe_{86.7}Cr_{4.4}Mo_{0.6}V_{1.1}W_{2.5}C_{4.7}$ alloy after deep etching. The illustrated 3-dimensional skeleton-like structure of the complex carbides has formed between the retained austenite and the martensite. This hard and finely ramified carbide network distributed throughout the entire ingot is a specific characteristic of this alloy and important for its mechanical properties.

The combination of the high-strength phases martensite and carbides leads to a high macrohardness of 61 ± 0.6 HRC, which is very similar to that of high speed tool steels [6].

Figure 3 shows the engineering compressive stress and the volume fraction of martensite as a function of the engineering strain for the as-cast material. The most significant mechanical property of the present $Fe_{86.7}Cr_{4.4}Mo_{0.6}V_{1.1}W_{2.5}C_{4.7}$ alloy is its very pronounced work-hardening behaviour. The material starts to deform plastically at a 0.2-offset yield strength of 1296 ± 10 MPa and fails at an outstanding engineering compression ultimate strength of 5439 ± 20 MPa at a compression strain of 23 ± 0.5%, which is much superior compared with commercial HSS [8]. In order to clarify the reason for this special deformation behaviour, the volume fraction of martensite at different strain levels (0, 4, 9, 14 and 24%) was determined (Fig. 3). The volume fraction of martensite in the examined iron-based alloy clearly increases with increasing strain. The metastable austenite in the as-cast material, which amounts to about 30 vol.% (when the volume fraction of carbides is neglected), transforms into martensite because of the imposed external stress during deformation. Therefore, the reason for the large work hardening is, besides conventional deformation mechanism like, e.g. solid solution strengthening, particle strengthening or grain boundary hardening, linked with the TRIP effect caused by the deformation-induced transformation of metastable austenite into martensite [12, 14, 23, 24].

SEM has been used to analyze the failure behaviour of the alloy. Figure 4a presents the typical microstructure of a fractured compression test sample. The fracture always occurred in the direction of the major shear stress, i.e. at an angle of about 45°, so that a typical shear fracture appears. Apart from dimples distorted in the direction of slip (not shown here), the fracture surface reveals partially melted zones due to the high deformation energy and the large heat release upon fracture (Fig. 4a).

Besides compression tests, also room temperature tensile tests were performed. Upon tensile loading the $Fe_{86.7}Cr_{4.4}Mo_{0.6}V_{1.1}W_{2.5}C_{4.7}$ alloy exhibits a high 0.2-yield strength of 618 ± 10 MPa and an ultimate tensile strength (UTS) of 972 ± 32 MPa at a total strain after break (A_t) of 1.1 ± 0.1% in the as-cast state. Furthermore, a certain amount of work hardening is detectable. Concerning the tensile yield and UTS stresses, the alloy can be considered as an ultra-high-strength alloy [3] and shows somewhat better tensile strength than as-cast HSS steels with similar compositions [25]. However, the ductility of the $Fe_{86.7}Cr_{4.4}Mo_{0.6}V_{1.1}W_{2.5}C_{4.7}$ alloy under tensile load is rather low, which can mainly traced back to the hard and brittle carbide network [5, 25] and also the high-strength martensitic phase in the as-cast state may have a certain influence [26, 27]. This behaviour of the investigated alloy under tensile stress is also reflected in the fracture features: all examined samples displayed brittle fracture, and the fracture occurred perpendicular to the maximum tensile stress, so a typical cleavage fracture appears. The failure mainly occurs at the interface between the hard and brittle

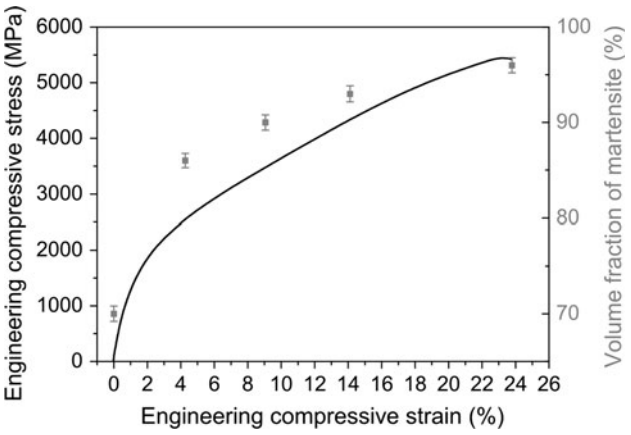

Fig. 3 Engineering compressive stress and volume fraction of martensite as a function of the engineering strain for the as-cast $Fe_{86.7}Cr_{4.4}Mo_{0.6}V_{1.1}W_{2.5}C_{4.7}$ alloy

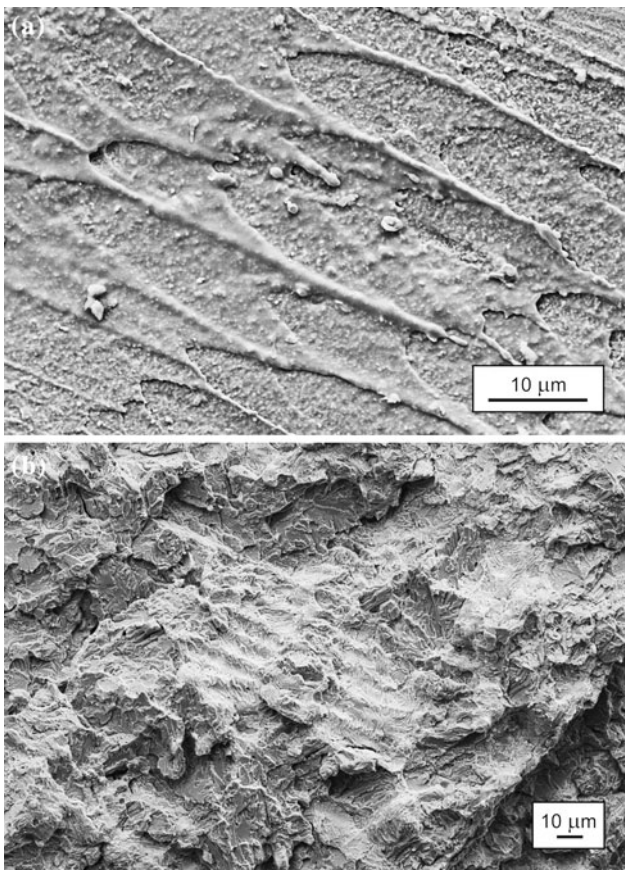

Fig. 4 **a** SEM image of the fracture surface of a compression test sample showing partial melting; **b** SEM image of the fracture surface of a tensile test sample displaying a removed dendrite

carbides and the dendrites (Fig. 4b). Besides the carbide network, micropores, which cannot be completely avoided in a cast material, promote enhanced crack propagation, because under tensile loading the crack grows perpendicular to the applied force, which leads to an additional crack opening and a failure at low overall tensile strain.

Comparing the deformation behaviour under tensile and compressive loading reveals that the yield strength under uniaxial compression is much higher than under uniaxial tension. This difference in the flow behaviour has been termed strength differential (SD) effect [28] and was earlier observed and investigated by Chait [29] and Hirth and Cohen [28] for martensitic steels. Hirth and Cohen [28] also gave some tentative explanations of the SD phenomenon. The difference in yield strength under uniaxial compressive and tensile loading could, for example, traced back to residual stresses arising from the volume expansion of the martensitic transformation or to internal cracking as a result of the high hardness of the $Fe_{86.7}Cr_{4.4}Mo_{0.6}V_{1.1}W_{2.5}C_{4.7}$ alloy [28]. In fact, flaws which are already present in the as-cast material or that are induced during testing (for example crack formation at carbides), are more detrimental in tension than in compression, and have therefore to be minimised for obtaining excellent mechanical properties. Appropriate measures to circumvent this problem will be subject of future investigations.

Conclusions

A $Fe_{86.7}Cr_{4.4}Mo_{0.6}V_{1.1}W_{2.5}C_{4.7}$ ultra-high-strength alloy was manufactured under special preparation conditions, which promote a microstructure composed of martensite, retained austenite and a fine network of special carbides already in the as-cast state. The combination of high-strength phases with ductile austenite yields an alloy with outstanding mechanical properties. The alloy exhibits a high macrohardness as well as extremely high engineering compression strength combined with large compression strain and a strong work-hardening behaviour. The reason for performance can be traced back to the successive transformation of the retained austenite into martensite during deformation, as confirmed by the considerably increasing volume fraction of martensite with increasing compression strain. Furthermore, the alloy shows a high tensile yield stress and UTS already in the as-cast condition. The quasi-static compression and tensile tests reveal a significant difference in the mechanical behaviour under the different loading conditions. Shear fracture occurs under compression, whereas cleavage dominates for tensile loading. For further clarification of the fracture mechanisms and the crack imitation and propagation in the present alloy, fracture mechanical tests have to be performed in the future.

In conclusion, the $Fe_{86.7}Cr_{4.4}Mo_{0.6}V_{1.1}W_{2.5}C_{4.7}$ alloy offers a wide range of applications already in the as-cast condition due to its ultra-high compression strength and ductility and even high strength under tensile loading. Therefore, the material has a large potential to replace currently used high performance steels for the automotive and tool manufacturing industry in the future.

Acknowledgements The authors are grateful to H. Bußkamp, M. Frey, W. Gruner, R. Keller, H. Klauß, S. Roth, A. Voß and H. Wendrock for technical assistance and valuable discussions. This study was supported by the European Union and the Free State of Saxony (SAB grant no. 13853/2379 and 13795/2379) in the framework of the European Centre for Emerging Materials and Processes Dresden (ECEMP).

References

1. Sugimoto KI, Muramatsu T, Hashimoto SI, Mukai Y (2006) J Mater Process Technol 177:390
2. Mori K, Akita K, Abe Y (2007) Int J Mach Tools Manuf 47:321
3. Möller E (2008) Handbuch der Konstruktionswerkstoffe. Carl Hanser Verlag, München
4. Pawlak SJ, Krztoń HJ (2009) J Arch Mater Manuf Eng 36:18
5. Hwang EC, Lee S, Lee HC (1998) Mater Sci Eng A 254:296
6. Hwang EC, Lee S, Lee HC (1998) Mater Sci Eng A 254:282
7. Park JW, Lee HC, Lee S (1999) Metall Mater Trans A 30:399
8. Brar NS, Hari Manoj Simha C (2000) J Phys 10:611
9. Xu W, Rivera-Díaz-del-Castillo PEJ, Wang W, Yang K, Bliznuk V, Kestens LAI, van der Zwaag S (2010) Acta Mater 58:3582
10. Fu H, Qu Y, Xing J, Zhi X, Jiang Z, Li M, Zhang Y (2008) JMEPEG 17:535
11. Nadeinskaya EP, Badaeva AA (1961) Metal Sci Heat Treat 3:38
12. Hufenbach J, Kühn U, Krüger L, Wendrock H, Eckert J (2010) Steel Res Int 82:51
13. Kühn U, Mattern N, Gemming T, Siegel U, Werniewicz K, Eckert J (2007) APL 90: 261901/1-3
14. Kühn U, Romberg J, Mattern N, Wendrock H, Eckert J (2010) J Mater Res 25:368
15. Srivastava RM, Eckert J, Löser W, Dhindaw BK, Schultz L (2002) Mater Trans 43:1670
16. Rietveld HM (1969) J Appl Cryst 2:65
17. Roisnel T, Rodriguez-Carvajal J (2001) Mater Sci Forum 118:378
18. Kohlhaas R, Duenner P, Schmitz-Pranghe N (1967) Z Angew Phys 23:245
19. Ridley N, Stuart H (1970) Met Sci J 4:219
20. Page K, Li J, Savinelli R, Szumila HN, Zhang J, Stalick JK, Proffen T, Scott SL, Seshadri R (2008) Solid State Sci 10:1499
21. Harsta A, Rundqvist S, Thomas JO (1978) Acta Chem Scand A 32:891
22. Khaenko BV, Gnitetskii OA, Kublii VZ (1991) Dopov Akad Nauk Ukr RSR 3:78
23. Powell GW, Marshall ER, Backofen WA (1958) Trans ASM 50:478
24. Evans JT, Rawlings R (1969) Mater Sci Eng 4:297
25. Benazza A, Ziadi A, Serier B, Bouiadjra BB, Boutabout B (2007) J Mater Sci 42:834. doi:10.1007/s10853-006-0075-y
26. Fahr D (1971) Metall Mater Trans B 2:1883
27. Kumar A, Singh SB, Ray KK (2008) Mater Sci Eng A 474:270
28. Hirth JP, Cohen M (1970) Metall Trans 1:3
29. Chait R (1972) Metall Trans 3:365